Simulations of Subnanometer Scale Image Contrast in Atomic Force Microscopy of Self-Assembled Monolayers in Water

José Cobeña-Reyes, Tao Ye, and Ashlie Martini*

Cite This: *Chem. Biomed. Imaging* 2023, 1, 147−156

Read Online

ACCESS | Metrics & More | Article Recommendations | Supporting Information

ABSTRACT: Achieving high-resolution images using dynamic atomic force microscopy (AFM) requires understanding how chemical and structural features of the surface affect image contrast. This understanding is particularly challenging when imaging samples in water. An initial step is to determine how well-characterized surface features interact with the AFM tip in wet environments. Here, we use molecular dynamics simulations of a model AFM tip apex oscillating in water above self-assembled monolayers (SAMs) with different chain lengths and functional groups. The amplitude response of the tip is characterized across a range of vertical distances and amplitude set points. Then relative image contrast is quantified as the difference of the amplitude response of the tip when it is positioned directly above a SAM functional group vs positioned between two functional groups. Differences in contrast between SAMs with different lengths and functional groups are explained in terms of the vertical deflection of the SAMs due to interactions with the tip and water during dynamic imaging. The knowledge gained from simulations of these simple model systems may ultimately be used to guide selection of imaging parameters for more complex surfaces.

KEYWORDS: *dynamic atomic force microscopy, image contrast, self-assembled monolayers, solid−liquid interfaces, molecular dynamics simulation*
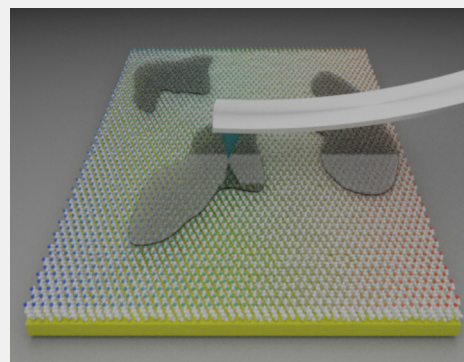
INTRODUCTION

The understanding of solid−liquid interfaces is relevant to multiple phenomena, including wettability,[1] lubrication,[2] protein stability,[3] pharmaceutical development,[4] as well as electrochemical energy storage/conversion devices such as batteries,[5] supercapacitors,[6] and fuel cells.[7,8] In situ microscopy techniques, such as atomic force microscopy (AFM), are widely used to study these phenomena due their versatility and ability to image samples in liquid media.[9−11] Although the lateral resolution of AFM in liquid is typically limited to nanometers, the development of noncontact AFM, that minimizes the deformation of the tip−sample contact through careful regulation of tip−sample interactions, has enabled AFM to achieve subnanometer lateral resolution for some organic thin films as well as minerals in water.[12,13] To resolve subnanometer scale features, there must be contrast at this length scale, i.e., the AFM should yield different signals at different surface sites. However, our understanding of how atomic scale interactions between the tip apex, the solvent, and the surface ultimately determine the subnanometer scale image contrast remains very limited. For instance, it is not entirely clear whether different chemical functional groups yield different image contrast and, if they do, what interactions are responsible for that difference. These questions need to be answered for subnanometer resolution AFM to serve as a powerful chemical imaging technique of solid−liquid interfaces.

The primary challenge with understanding contrast mechanisms lies in the difficulty of understanding the interactions between the tip, water, and sample.[14] When samples are immersed in water, tip−sample, tip−water, and water−sample forces affect the dynamic response of the cantilever. For instance, water tends to form hydration layers next to the surface being imaged, which affects the subnanometer scale imaging[15,16] due to several phenomena: confinement of the layers between tip and sample,[17−19] displacement of the layers by the motion of the tip,[20,21] and in some cases, stabilization of the layers by hydrogen bonding between water and sample.[15]

One approach to investigating contrast mechanisms in AFM is molecular dynamics (MD) simulation.[14,22,23] MD simulations capture atomic scale interactions, but are computationally inexpensive, which allows modeling large and complex systems, as well as the dynamic aspects of the AFM measurement. For example, experimental contrast patterns of calcite in water were reproduced using MD simulations with variable tip−sample distance and driving amplitude.[23] Another material system for
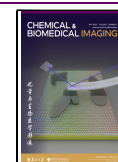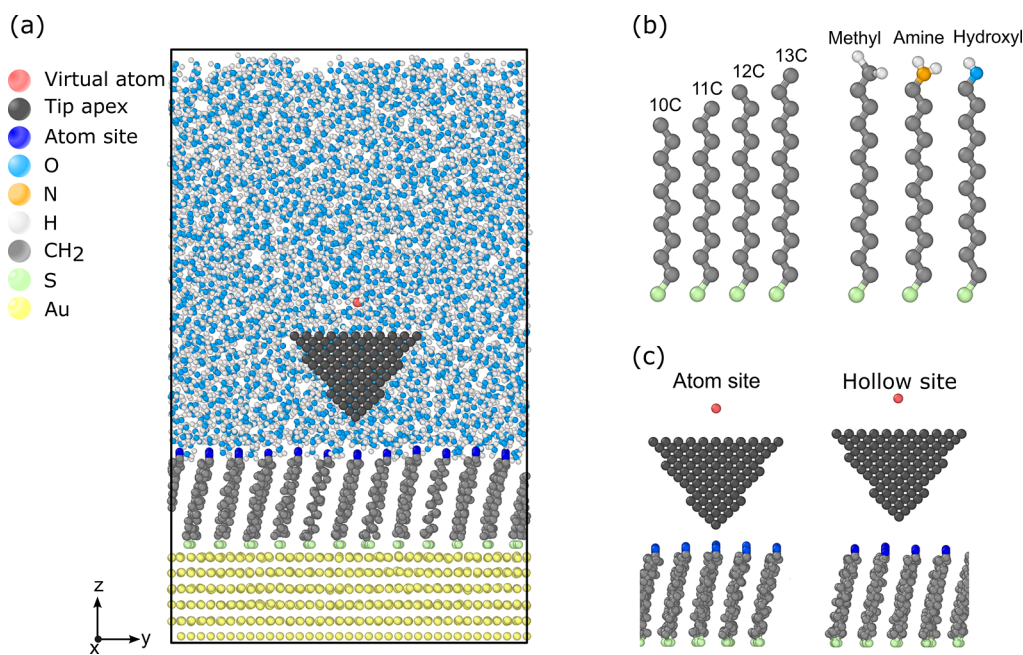
Figure 1. (a) Cross-sectional view of the MD model comprising an Au(111) substrate, SAMs, tip, virtual atom, and water molecules. (b) SAM molecules with different functional groups and chain lengths used in the models. (c) Close-up snapshots of models shown without the water where the tip is positioned at an atom or hollow site.

investigating the subnanometer contrast mechanisms of solid—liquid interfaces, and the one we focus on here, is alkanethiol self-assembled monolayers (SAMs). SAMs are widely used in a variety of technological applications for sensing,[24] tribology,[25] and biointerfaces,[26] but are also ideal model systems due to their simplicity and tunable chain lengths and functional groups. One study used MD simulations to investigate how tip interactions with SAMs at different lateral positions affected image contrast in vacuum.[22] Our previous study simulated AFM on a hydroxyl terminated SAM and showed that contrast on SAMs in water strongly depended on interactions with both the sample and the water.[14] Here, we used MD simulations of an AFM tip apex and SAMs immersed in water to investigate the effect of surface functional groups and chain length on subnanometer scale image contrast. We modeled different chain lengths, from 10 to 13 carbons, and three functional groups, methyl ($-CH_3$), amine ($-NH_2$), and hydroxyl ($-OH$). Additionally, we simulated the variation of contrast with many different combinations of tip—SAM distances and driving amplitudes. The effects of SAM chain length and functional group were analyzed and the deflection of the chains during imaging was identified as the key factor determining image contrast. These results provide insight into the effect of chemical and structural sample features on the operating parameters required to achieve subnanometer resolution in water. The atomic insight into how functional groups and chain lengths determine contrast presented here can also be helpful to assess AFM images of other organic samples in liquid.

■ MODELS AND METHODS

A cross-sectional view of the model is shown in Figure 1a. Twelve different $S(CH_2)_nX$ SAMs were modeled, where X is methyl, amine, or hydroxyl and n is 10, 11, 12, or 13. Illustrations of individual SAM molecules with different lengths and functional groups are shown in Figure 1b. The SAMs were placed on an atomically flat Au(111) surface with dimensions 50 Å × 50 Å in the x- and y-directions. The sulfur atoms were the head groups of the SAM chains and were placed such

that they formed a $(\sqrt{3} \times \sqrt{3})$ $R30$ structure on the gold surface. The AFM tip apex was modeled as diamond in a conical shape; select simulations were also run with conical silicon tip with a silanol group at the apex (section S6). The height of the tip was 12 Å, and the radius of the upper base of the tip was 9 Å. The sharp tip geometry reflects the assumption that interactions at a few atoms at the end of the tip apex are the most relevant to atomic contrast.[27] The space between the top of the SAMs and the upper boundary of the simulation box (6 nm) was filled with water molecules such that the density at 300 K was 0.999 g/cm^3.

We used the OPLS united-atom force field optimized for longer hydrocarbon chains[28] to model the body of the SAM molecules, where the hydrogen atoms are treated implicitly with their masses added to the corresponding carbon atom. The terminal functional groups were modeled using the OPLS all-atom potential[29] for more accurate interactions between the SAMs and the water or tip. The thiol—Au interactions were modeled using the Morse potential.[30,31] The water molecules were simulated with the SPC/E rigid model.[32] The tip was modeled using the adaptive intermolecular reactive empirical bond order (AIREBO)[33] potential and the embedded atom method (EAM)[34] was employed to model the Au substrate. The Lennard-Jones potential and the Lorentz—Berthelot mixing rules were used for all other nonbonded interactions. The tip was treated as a rigid body and the bottom 10 Å of the Au substrate was kept fixed. Periodic boundary conditions were set in all dimensions. All the simulations were run using the LAMMPS package[35] in the NVT ensemble at 300 K with a time step of 0.25 fs. The visualization of structures was performed using Ovito software.[36]

Independent simulations were run with the tip positioned at atom and hollow sites, identified in Figure 1c. The atom site is located directly above the functional group of a SAM chain and the hollow site corresponds to the empty space between two adjacent chains. We choose these two sites because recent studies[14,37−39] have shown that image contrast can be quantified by the difference in the tip's response amplitude at these positions. The tip was connected to a virtual atom, mimicking the cantilever, through a harmonic spring with a stiffness of 40 N/m. This spring constant was used to mimic a stiff cantilever used in existing subnanometer resolution imaging studies,[40] although a subset of the simulations were also run with a spring constant of 4 N/m (section S6). A relaxation step that took 1 ns was used to ensure that the
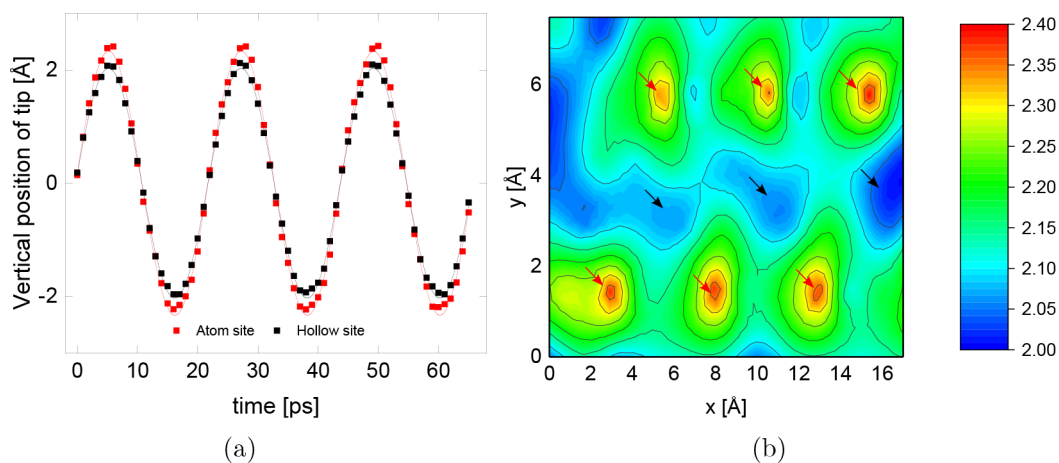
Figure 2. (a) Representative plots of tip position vs time at the atom (red) and hollow (black) sites from a simulation of 12C SAMs-NH$_2$ at a tip−sample distance of 1 Å and driving amplitude of 3 Å. Lines are sinusoidal fits to the simulation data. Contrast is defined as the difference in the response amplitude of the tip at the atom and hollow sites. (b) Map showing the amplitude of the tip at different lateral positions where color indicates contrast in units of Å. Red and black arrows identify representative atom and hollow sites, respectively.
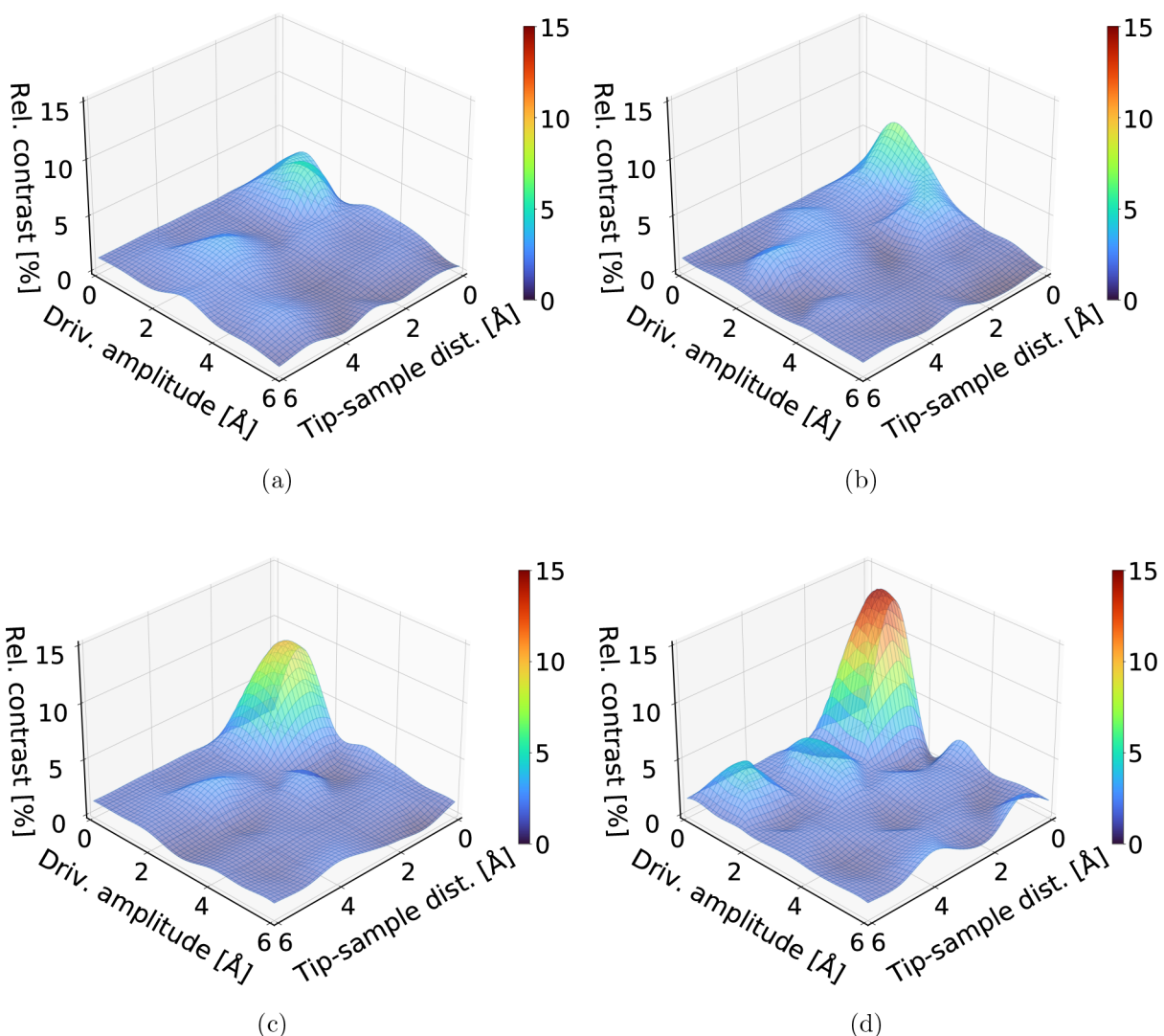

Figure 3. Representative contour plots showing the relative contrast for SAMs (a) −CH$_3$ with 11C, (b) −OH with 11C, (c) −NH$_2$ with 11C, and (d) −NH$_2$ with 13C. Taller peaks and red color in the contours indicate higher image contrast.

system reached 300 K. Once the system was relaxed, the virtual atom was oscillated in the z direction at a frequency of 91 GHz and a set driving amplitude, causing the tip to oscillate. The center of mass of the tip motion was recorded every 1 ps. Simulations were run at a range of
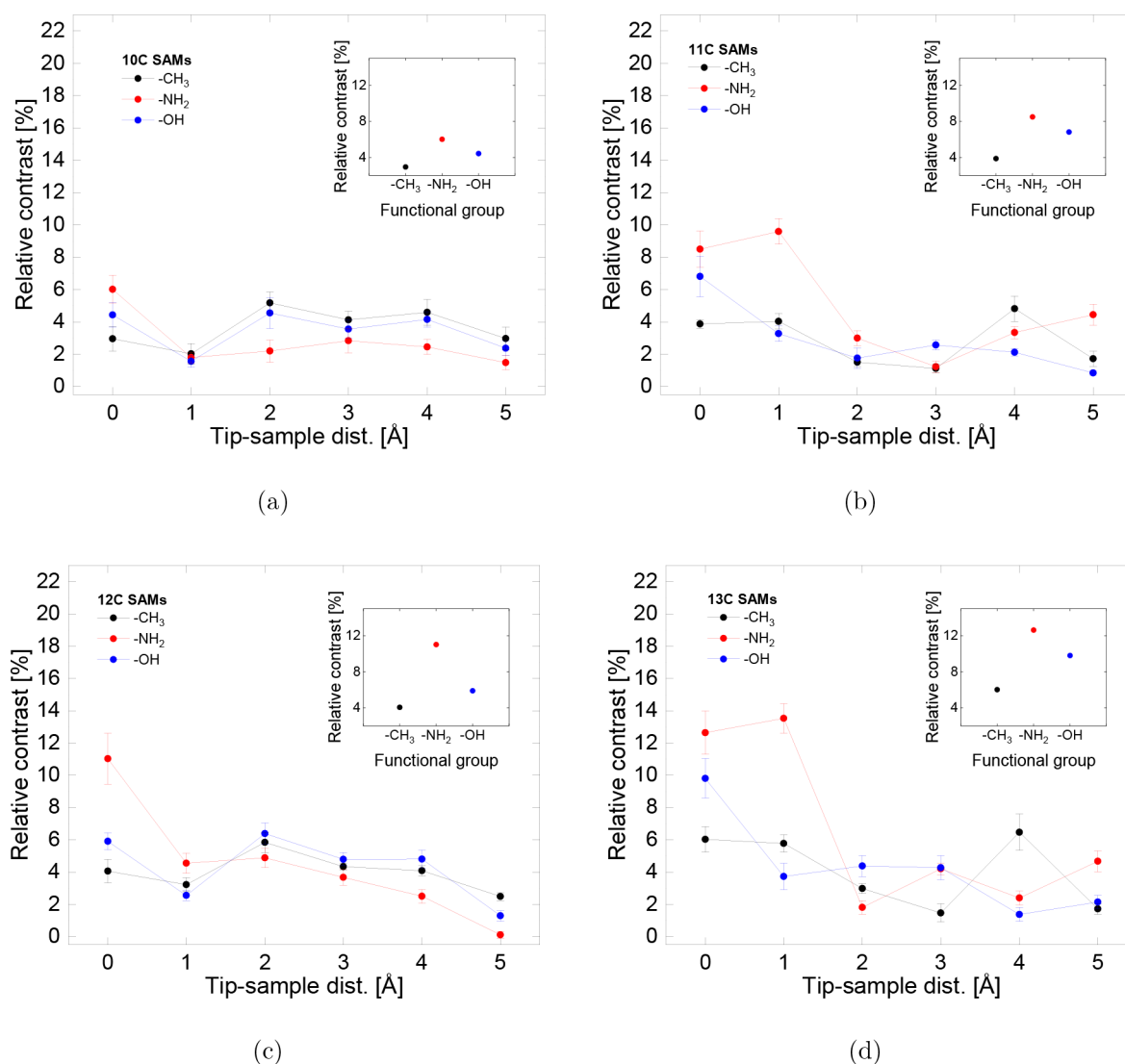
Figure 4. Relative contrast as a function of tip−sample distance at an amplitude of 1 Å for SAM chain lengths of (a) 10C, (b) 11C, (c) 12C, and (d) 13C. The insets show the data plotted vs functional group at a tip−sample distance of 0 Å. The error bars are the standard error of the mean from three independent simulations.

driving amplitudes from 1 to 6 Å and tip−SAM distances from 0 to 5 Å. The duration of the production stage was 1.0 ns. Three independent simulations were run for each SAM, chain length, tip−sample distance, and driving amplitude.

■ RESULTS AND DISCUSSION

Figure 2a shows representative simulation results where the tip response to the driving amplitude differs at the atom and hollow sites. The simulation data was fitted to a sinusoidal function to obtain the tip response amplitude. Figure 2b shows the fit tip amplitude response at different lateral positions on the SAMs surface. The difference between the fit amplitude at the atom and hollow sites was used to quantify image contrast. We next calculated relative image contrast as the difference between the response amplitudes at the atom and hollow sites divided by the driving amplitude, expressed as a percentage. This quantity gives the contrast per unit driving amplitude applied. This definition of contrast is useful for practical applications, particularly for biological and soft samples for which it is desirable to maximize contrast with the smallest possible driving amplitude to

minimize the effect of long-range interactions between the tip and water.[41]

Simulation results like those in Figure 2a were obtained at a range of tip−sample distances and driving amplitudes for 12 combinations of SAM terminal groups and chain lengths. From these, contour plots of the relative contrast, averaged over three independent simulations, were generated. Representative examples are shown in Figure 3, and the other eight contour plots can be found in Figures S1−S3. These figures show relative contrast on the z-axis plotted against tip−sample distance on the x-axis and driving amplitude on the y-axis. Generally, relative contrast is higher at small amplitudes and distances in all cases. This trend is consistent with what is observed experimentally. Small values of amplitude are used for subnanometer resolution imaging because they minimize the effect of the nonlinear long-range forces and increase the sensitivity to short-range forces.[42,43] Small amplitudes are achieved in practice when using low-noise stiff cantilevers, like the one modeled here, that can help suppress thermal noise, allowing detection of small forces.[44]
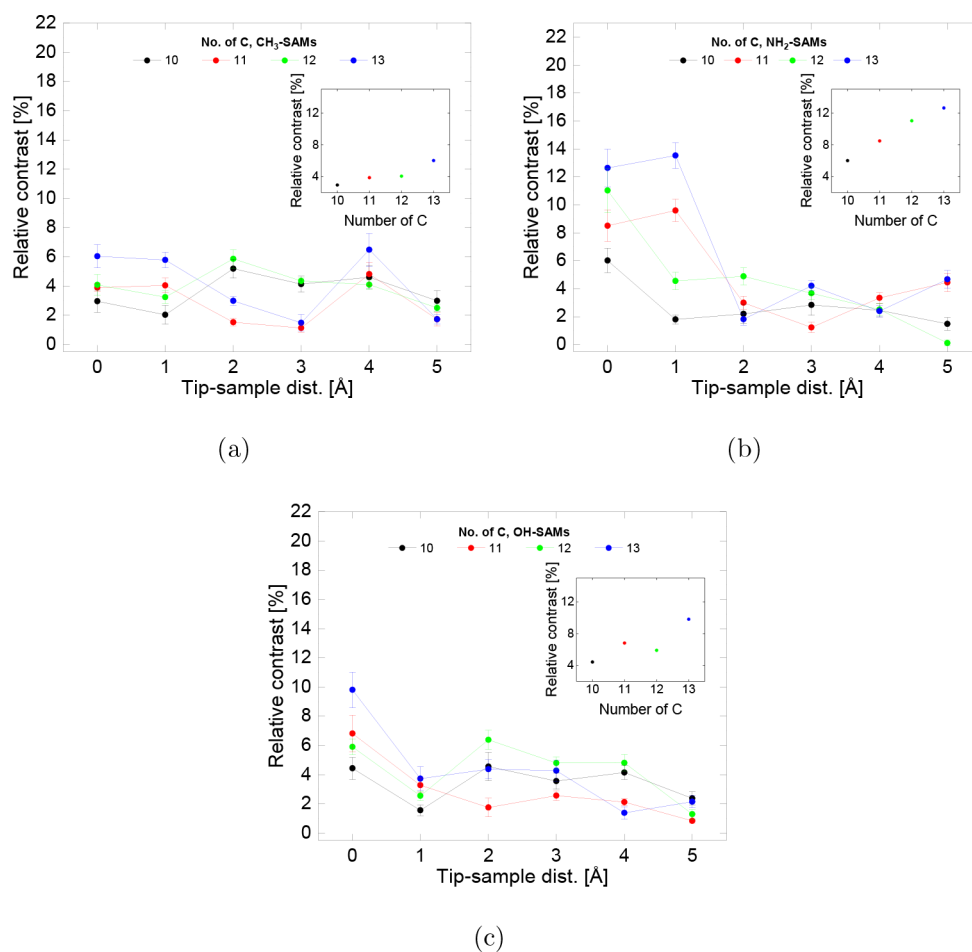
(a)

(b)

(c)

Figure 5. Relative contrast as a function of tip–sample distance at an amplitude of 1 Å for functional groups (a) −CH₃, (b) −NH₂, and (c) −OH. The insets show the data plotted vs chain length at a tip–sample distance of 0 Å. The error bars are the standard error of the mean from three independent simulations.
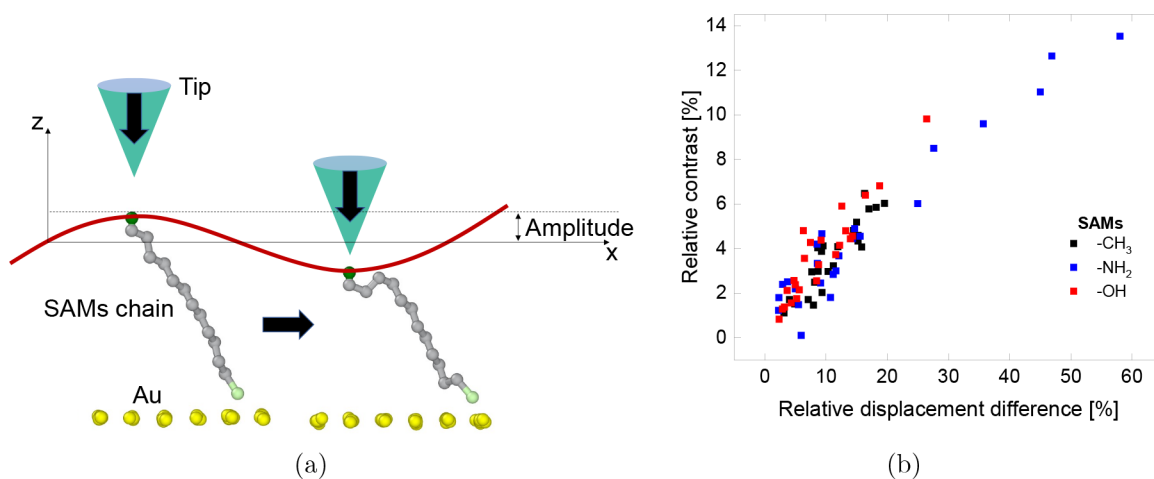

(a)

(b)

Figure 6. (a) Schematic of the calculation of functional group amplitude used to determine the relative displacement difference of the functional groups at the atom and hollow sites. (b) Relative contrast vs relative displacement difference for all functional groups and chain lengths at a tip–sample distance of 0 Å and amplitude of 1 Å.

To isolate the effect of the functional group, relative contrast is plotted vs tip–sample distance at a fixed amplitude of 1 Å in Figure 4, where each plot contains data for thiolate SAMs with the same chain length but different terminal functional groups. At small tip–sample distances, where the relative contrast is highest, the relative contrast follows the order: −NH₂ > −OH >

−CH₃. This same trend was observed with a smaller spring constant and different model tip material (section S6).

Then to analyze the trend of chain length, the relative contrast at an amplitude of 1 Å is replotted in Figure 5 with each plot corresponding to SAMs with the same terminal functional groups but different chain lengths. At small tip–sample
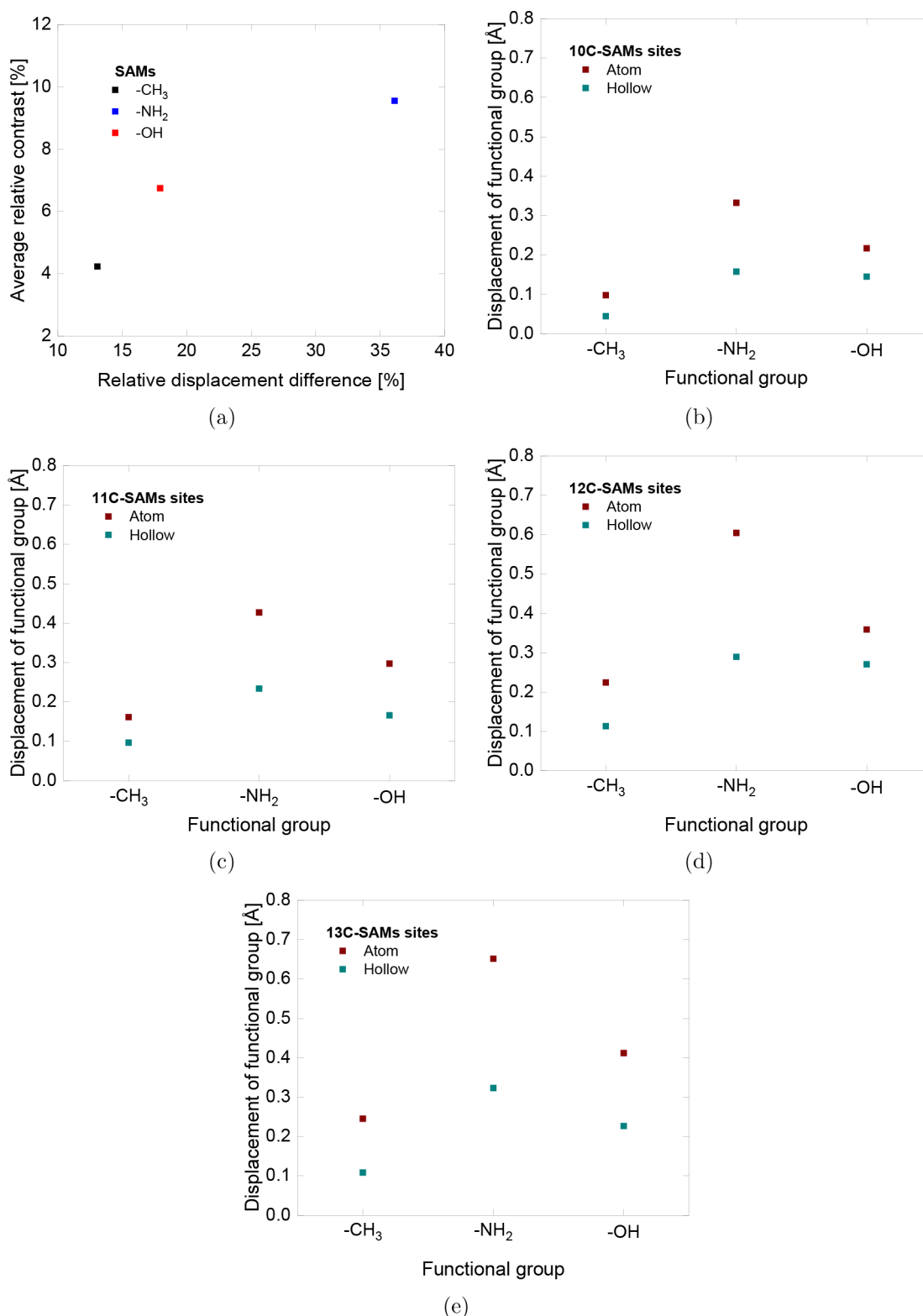
Figure 7. (a) Relative contrast vs relative displacement difference averaged over all four chain lengths for each functional group at tip−sample distance 0 Å and driving amplitude 1 Å. Functional group displacement in response to tip oscillation at the atom and hollow sites for (b) 10C, (c) 11C, (d) 12C, and (e) 13C SAMs.

distances, we consistently observe the highest contrast for the 13C SAMs and the lowest for the 10C SAMs. However, there also appear to be odd−even effects that depend on the functional group. For instance, for the SAMs-OH shown in Figure 5c, contrast follows the trend 13C > 11C > 12C > 10C, whereas for the SAMs-NH$_2$ in Figure 5b, the order is 13C > 12C > 11C > 10C. The trends with respect to chain length were also observed for the different spring constant and tip material models (section S6).
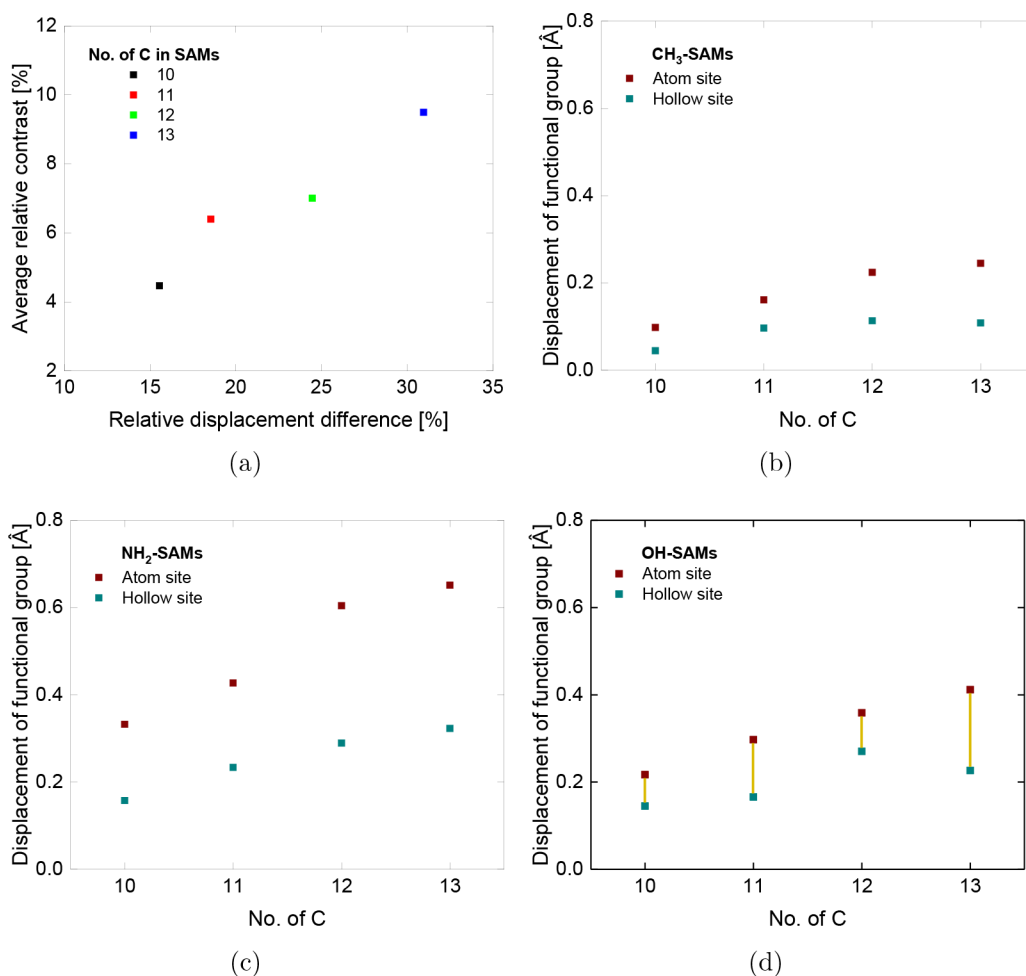
Figure 8. (a) Relative contrast vs relative displacement difference averaged over all three functional groups at each chain length. The averages were taken at tip−sample distance 0 Å and driving amplitude 1 Å. Functional group displacement in response to tip oscillation at the atom and hollow sites for SAMs (b) −CH$_3$, (c) −NH$_2$, and (d) −OH. Yellow lines in (c) highlight the difference in displacement between atom and hollow sites.

To understand the trends with respect to chain length and functional groups, we calculated various parameters from the simulations. We calculated the total, SAM, and water potential energies, as well as the position and local displacement of the water, when the tip oscillated above an atom or hollow site. None of these was found to be correlated to the relative contrast trends. However, trends similar to image contrast were observed for the deflection of the SAM molecules in response to interactions with the tip, specifically, the difference between the vertical displacement of the SAM functional groups when the tip oscillated at the atom vs the hollow site. To quantify this displacement, we fitted the motion of the heaviest atom in the functional group of the SAMs (C for −CH$_3$, N for −NH$_2$, and O for −OH) to a sinusoidal function, as illustrated schematically in Figure 6a. The displacement at atom sites was computed from the amplitude of the heavy atom in the functional group above which the tip oscillated; for the hollow sites, it was the average of the amplitudes of the two functional groups on either side of the position of the tip oscillation. Then the difference between the functional group amplitudes at the atom site and the hollow site was divided by driving amplitude to calculate the relative displacement difference expressed as a percentage.

The correlation between relative contrast and functional group relative displacement difference is shown in Figure 6b. Despite the scatter in the data, there is a consistent trend of

contrast increasing with displacement difference, indicating that a key factor in determining image contrast is the deflection of the SAM molecules in response to interactions with the tip at the atom and hollow sites. We analyzed the SAM chain displacement at the atom and hollow sites separately and found that the atom site displacement was always greater than the hollow site displacement. Therefore, a large relative displacement difference for a given case could be attributable to either less displacement at the hollow site or more displacement at the atom site. From the results in Figures 4 and 5, we found that relative contrast was affected by polarity of the functional group, chain length, and odd−even effects. We analyzed each of these factors in the context of relative displacement difference at the atom and hollow sites.

First, as shown in Figure 5, relative contrast follows the order −NH$_2$ > −OH > −CH$_3$, and the same trend is exhibited by the relative functional group displacement difference as shown in Figure 7a. The displacement at the atom and hollow sites is analyzed separately in Figure 7b−e, which shows that the difference between the functional groups is larger at the atom site than the hollow site, indicating the contrast trend is attributable to interactions at the atom sites. We hypothesize that this difference is due to water molecules present between the functional group and tip, which differs for the different functional groups due to stronger interactions between water

molecules and functional groups. A parameter such as solubility provides an indication of the strength of the interactions between water and a molecule. The solubility of 10C-NH$_2$ is 0.55 g/L, higher than 0.037 g/L for 10C-OH and 0.009 g/L for 10C-CH$_3$; the same trend is exhibited by SAMs of other lengths (as long as there are more than six C).[45] Solubility is correlated to the position of the water layer that forms next to the surface where, as shown in Figure S4, the first water layer was closest to the functional group for −NH$_2$ and furthest for −CH$_3$.

To understand the effect of water binding on functional group displacement, we computed the total force in the vertical direction between the SAMs and the tip and water molecules, at the atom and hollow sites separately. The largest force was observed for the SAMs-NH$_2$, as shown in Figure S5, likely due to the dense water layer closest to these SAMs. Tracking the number of water molecules confined between tip and sample showed there was more water at the atom than the hollow sites (Figure S6), consistent with the larger force difference (Figure S5) and displacement (Figure 7) at the atom sites. Therefore, the contrast trend is correlated with interactions between the functional groups and the water molecules, where a more tightly binding water layer will increase the force the tip experiences more at the atom site than the hollow site, thereby increasing the difference in displacement at these sites and, in turn, tip amplitude contrast. This explanation is further supported by the results from simulations with a silanol-terminated silicon tip (section S6) which had stronger interactions with water than the diamond which led to more water between the tip and SAM atom sites and, in turn, higher contrast.

Next, we consider the effect of the length of SAM chain on contrast. In Figure 5, for all three functional groups, 13C chains have higher contrast than 10C carbon chains. Figure 8a shows that the average of the relative displacement differences for the three functional groups at tip−sample distance 0 Å and amplitude 1 Å is largest for 13C chains and smallest for 10C chains, consistent with the contrast trend. We hypothesize that low contrast is found for short chains because the shorter chain length leads to weaker interactions between the chains. With weaker chain packing, the SAMs are more disordered, i.e., more liquid-like.[28,46,47] Specifically, the response of small, liquid-like chains to tip oscillation is less sensitive to the lateral position of the tip with respect to the functional group. To test this hypothesis, we plotted the functional group displacement as a function of number of carbon in Figure 8b−d. In all cases, the displacement of the functional group at both the atom and hollow sites increases with chain length. However, the increase is not as a dramatic at the hollow sites. As a result, the difference between the relative displacement of the functional groups at the atom and that at the hollow sites is smaller for 10C chains than 13C chains, supporting the hypothesis that the liquid-like behavior of short chains may explain their lower image contrast.

At the smallest tip−sample distances, the effect of chain length is monotonic for the SAMs-CH$_3$ and SAMs-NH$_2$. However, as shown in Figure 5c, the contrast for the SAMs-OH follows the order 10C < 12C < 11C < 13C, indicating an odd−even effect. Properties of SAMs are known to depend on whether the number of C atoms is odd or even. For instance, odd−even configurations have been reported to affect water contact angle[1] and change the wettability of the SAMs chain. Other studies have shown that properties such as the friction coefficient differ between odd and even SAMs chains.[48] Odd−even behavior is also seen in our results for SAMs-OH, where the difference between the displacement at the atom and hollow sites is larger

for odd numbers of carbon atoms (yellow lines in Figure 8d). We hypothesize that even chains have lower contrast because the displacement at the hollow sites is reduced by the formation of hydrogen bonds between the functional groups. The arrangement of the atoms in the −OH functional group in 11C and 12C chain is shown in Figure S7. To quantify hydrogen bonds in the simulations, we used the geometric criteria based on bond lengths and angles[49] when the tip was far from the SAMs. The average number of hydrogen bonds per chain in the even SAMs-OH was 1.6 ± 0.14 and 1.4 ± 0.17 for the 10C and 12C cases, whereas in the odd SAMs-OH, 11C and 13C, it was 0.6 ± 0.19 and 0.3 ± 0.11. The O−H bonds of the hydroxyl terminal groups of alkanethiolate SAMs with an even number of carbon atoms in the alkyl chains are more parallel to the surface than those with an odd number of carbon atoms. A more parallel orientation favors interchain hydrogen bonding as shown in Figure S7. The presence of hydrogen bonds has been reported[50] in SAMs with an even number of C atoms and hydrophilic functional groups. More interchain hydrogen bonding results in smaller displacement when the tip is between two chains at hollow sites, while having little effect on displacement at atom sites. This results in smaller relative displacement difference and lower contrast for SAMs-OH with even numbers of C atoms.

■ CONCLUSIONS

MD simulations were used to mimic dynamic AFM imaging in water of model systems of SAMs with four different chain lengths (10C, 11C, 12C, and 13C) and three functional groups (methyl, amine, and hydroxyl) to understand how these variables affect image contrast. Contrast was quantified from the amplitude response of the tip at atom and hollow sites. Several combinations of driving amplitude and tip−sample distance were simulated and, in most cases, high contrast was observed at small distances and amplitudes. At the highest contrast conditions, the simulations showed several key trends that were found to be correlated to the deflection of the functional groups in response to interactions with the tip and the water molecules interaction with the functional groups. First, differences in the interactions between water and SAMs, quantified by solubility, affected the position of the water layer adjacent to the SAM surface, which changed the number of water molecules present between the tip and the sample and therefore the force experienced by the tip. A greater binding strength corresponded to more water molecules at atom sites which led to larger force and displacement difference at atom and hollow sites, and therefore higher contrast. Second, contrast generally increased with chain length, and was consistently higher for 13C chains than 10C chains for any SAM functional group. This was explained by the liquid-like behavior of shorter chains that caused their displacement response to the tip to be similar at hollow and atom sites, thereby decreasing contrast. Lastly, for the hydrophilic SAMs-OH, odd−even effects were reported, where chains with even numbers of C atoms had lower contrast than those with odd numbers of C atoms. This was explained by stronger interchain hydrogen bonding observed on even chains that decreased functional group displacement at hollow sites without affecting atom sites, decreasing contrast.

Broadly, this study showed the direct effect of replacing functional groups or changing chains lengths on subnanometer scale image contrast. While this study focused on contrast in amplitude signals, similar approaches may be developed to examine contrast in topographical height or frequency shift. Future studies that explore a more diverse array of functional

groups may reveal systematic trends that help us understand how different functional groups yield contrast at the subnanometer scale and how AFM can be used to discriminate between different functional groups on the same surface. We expect that the insights gained from these model systems with tailored surface functional groups and chain lengths to be relevant to imaging other soft and organic materials with subnanometer resolution. Finally, this study demonstrates the use of MD simulations for characterizing and understanding image contrast, and shows that MD can be an important tool for the scientific community to overcome the challenges inherent to high resolution AFM imaging of soft and organic materials.

■ ASSOCIATED CONTENT

Ⓢ Supporting Information

The Supporting Information is available free of charge at https://pubs.acs.org/doi/10.1021/cbmi.3c00001.

> Figures include eight relative contrast contour plots, water density profiles, average number of water molecules at atom and hollow sites, a schematic of hydrogen bonding between SAMs, and the results for different model tip and spring constant (PDF)

■ AUTHOR INFORMATION

Corresponding Author

Ashlie Martini − *Department of Mechanical Engineering, University of California Merced, Merced, California 95343, United States;* ⓞ orcid.org/0000-0003-2017-6081; Email: amartini@ucmerced.edu

Authors

José Cobeña-Reyes − *Department of Mechanical Engineering, University of California Merced, Merced, California 95343, United States;* ⓞ orcid.org/0000-0001-9677-4999

Tao Ye − *Department of Chemistry & Biochemistry, University of California Merced, Merced, California 95343, United States*

Complete contact information is available at:
https://pubs.acs.org/10.1021/cbmi.3c00001

Notes

The authors declare no competing financial interest.

■ ACKNOWLEDGMENTS

■ REFERENCES

(1) Ben Amara, F.; Dionne, E. R.; Kassir, S.; Pellerin, C.; Badia, A. Molecular origin of the odd−even effect of macroscopic properties of n-alkanethiolate self-assembled monolayers: bulk or interface? *J. Am. Chem. Soc.* **2020**, *142*, 13051−13061.

(2) Bresme, F.; Kornyshev, A. A.; Perkin, S.; Urbakh, M. Electro-tunable friction with ionic liquid lubricants. *Nat. Mater.* **2022**, *21*, 848−858.

(3) Zhang, S.; Chen, J.; Liu, J.; Pyles, H.; Baker, D.; Chen, C.-L.; De Yoreo, J. J. Engineering Biomolecular Self-Assembly at Solid−Liquid Interfaces. *Adv. Mater.* **2021**, *33*, 1905784.

(4) Khare, U.; Sharma, P.; Kumar, A. KA. Applications of surfactants in pharmaceutical formulation development of conventional and advanced delivery systems. *Int. J. Pharmacogn* **2019**, *6*, 155−63.

(5) McCaffrey, D. L.; Nguyen, S. C.; Cox, S. J.; Weller, H.; Alivisatos, A. P.; Geissler, P. L.; Saykally, R. J. Mechanism of ion adsorption to aqueous interfaces: Graphene/water vs. air/water. *Proc. Natl. Acad. Sci. U. S. A.* **2017**, *114*, 13369−13373.

(6) Lian, Z.; Chao, H.; Wang, Z.-G. Effects of confinement and ion adsorption in ionic liquid supercapacitors with nanoporous electrodes. *ACS Nano* **2021**, *15*, 11724−11733.

(7) Gohda, Y.; Schnur, S.; Groß, A. Influence of water on elementary reaction steps in electrocatalysis. *Faraday Discuss.* **2009**, *140*, 233−244.

(8) Yang, Y.; Xiong, Y.; Zeng, R.; Lu, X.; Krumov, M.; Huang, X.; Xu, W.; Wang, H.; DiSalvo, F. J.; Brock, J. D.; et al. Operando methods in electrocatalysis. *ACS Catal.* **2021**, *11*, 1136−1178.

(9) Guzman, H. V.; Perrino, A. P.; Garcia, R. Peak forces in high-resolution imaging of soft matter in liquid. *ACS Nano* **2013**, *7*, 3198−3204.

(10) García, R.; Perez, R. Dynamic atomic force microscopy methods. *Surf. Sci. Rep.* **2002**, *47*, 197−301.

(11) Jäggi, R. D.; Franco-Obregon, A.; Studerus, P.; Ensslin, K. Detailed analysis of forces influencing lateral resolution for Q-control and tapping mode. *Appl. Phys. Lett.* **2001**, *79*, 135−137.

(12) Garcia, R.; San Paulo, A. Attractive and repulsive tip-sample interaction regimes in tapping-mode atomic force microscopy. *Phys. Rev. B* **1999**, *60*, 4961.

(13) Solares, S. D.; Chawla, G. Frequency response of higher cantilever eigenmodes in bimodal and trimodal tapping mode atomic force microscopy. *Meas. Sci. Technol.* **2010**, *21*, 125502.

(14) Hu, X.; Yang, Q.; Ye, T.; Martini, A. Simulation of Subnanometer Contrast in Dynamic Atomic Force Microscopy of Hydrophilic Alkanethiol Self-Assembled Monolayers in Water. *Langmuir* **2020**, *36*, 2240−2246.

(15) Wu, J.; Wang, R.; Zhang, Y.; Chen, B.; Zhu, X. In situ scrutinize the adsorption of sulfamethoxazole in water using AFM force spectroscopy: Molecular adhesion force determination and fractiona-tion. *J. Hazard. Mater.* **2022**, *426*, 128128.

(16) Hu, X.; Nanney, W.; Umeda, K.; Ye, T.; Martini, A. Combined experimental and simulation study of amplitude modulation atomic force microscopy measurements of self-assembled monolayers in water. *Langmuir* **2018**, *34*, 9627−9633.

(17) Watkins, M.; Shluger, A. L. Mechanism of contrast formation in atomic force microscopy in water. *Phys. Rev. Lett.* **2010**, *105*, 196101.

(18) Watkins, M.; Berkowitz, M. L.; Shluger, A. L. Role of water in atomic resolution AFM in solutions. *Phys. Chem. Chem. Phys.* **2011**, *13*, 12584−12594.

(19) Reischl, B.; Watkins, M.; Foster, A. S. Free energy approaches for modeling atomic force microscopy in liquids. *J. Chem. Theory Comput.* **2013**, *9*, 600−608.

(20) Fukuma, T.; Higgins, M. J.; Jarvis, S. P. Direct imaging of lipid-ion network formation under physiological conditions by frequency modulation atomic force microscopy. *Phys. Rev. Lett.* **2007**, *98*, 106101.

(21) Kobayashi, K.; Liang, Y.; Amano, K.-i.; Murata, S.; Matsuoka, T.; Takahashi, S.; Nishi, N.; Sakka, T. Molecular dynamics simulation of atomic force microscopy at the water−muscovite interface: hydration layer structure and force analysis. *Langmuir* **2016**, *32*, 3608−3616.

(22) Bat-Uul, B.; Fujii, S.; Shiokawa, T.; Ohzono, T.; Fujihira, M. Molecular dynamics simulation of non-contact atomic force micros-copy of self-assembled monolayers on Au (111). *Nanotechnology* **2004**, *15*, 710.

(23) Tracey, J.; Miyazawa, K.; Spijker, P.; Miyata, K.; Reischl, B.; Canova, F. F.; Rohl, A. L.; Fukuma, T.; Foster, A. S. Understanding 2D atomic resolution imaging of the calcite surface in water by frequency modulation atomic force microscopy. *Nanotechnology* **2016**, *27*, 415709.

(24) Samanta, D.; Sarkar, A. Immobilization of bio-macromolecules on self-assembled monolayers: methods and sensor applications. *Chem. Soc. Rev.* **2011**, *40*, 2567−2592.

(25) Mate, C. M.; Carpick, R. W. *Tribology on the Small Scale: A Modern Textbook on Friction, Lubrication, and Wear*; Oxford University Press: New York, 2019.

(26) Faucheux, N.; Schweiss, R.; Lützow, K.; Werner, C.; Groth, T. Self-assembled monolayers with different terminating groups as model substrates for cell adhesion studies. *Biomaterials* **2004**, *25*, 2721−2730.

(27) Gross, L.; Mohn, F.; Moll, N.; Liljeroth, P.; Meyer, G. The chemical structure of a molecule resolved by atomic force microscopy. *Science* **2009**, *325*, 1110−1114.

(28) Siu, S. W.; Pluhackova, K.; Böckmann, R. A. Optimization of the OPLS-AA force field for long hydrocarbons. *J. Chem. Theory Comput.* **2012**, *8*, 1459−1470.

(29) Jorgensen, W. L.; Maxwell, D. S.; Tirado-Rives, J. Development and testing of the OPLS all-atom force field on conformational energetics and properties of organic liquids. *J. Am. Chem. Soc.* **1996**, *118*, 11225−11236.

(30) Mahaffy, R.; Bhatia, R.; Garrison, B. J. Diffusion of a butanethiolate molecule on a Au {111} surface. *J. Phys. Chem. B* **1997**, *101*, 771−773.

(31) Sung, I.-H.; Kim, D.-E. Molecular dynamics simulation study of the nano-wear characteristics of alkanethiol self-assembled monolayers. *Appl. Phys. A: Mater. Sci. Process.* **2005**, *81*, 109−114.

(32) Berendsen, H.; Grigera, J.; Straatsma, T. The missing term in effective pair potentials. *J. Phys. Chem.* **1987**, *91*, 6269−6271.

(33) Stuart, S. J.; Tutein, A. B.; Harrison, J. A. A reactive potential for hydrocarbons with intermolecular interactions. *J. Chem. Phys.* **2000**, *112*, 6472−6486.

(34) Grochola, G.; Russo, S. P.; Snook, I. K. On fitting a gold embedded atom method potential using the force matching method. *J. Chem. Phys.* **2005**, *123*, 204719.

(35) Thompson, A. P.; Aktulga, H. M.; Berger, R.; Bolintineanu, D. S.; Brown, W. M.; Crozier, P. S.; in't Veld, P. J.; Kohlmeyer, A.; Moore, S. G.; Nguyen, T. D.; et al. LAMMPS-a flexible simulation tool for particle-based materials modeling at the atomic, meso, and continuum scales. *Comput. Phys. Commun.* **2022**, *271*, 108171.

(36) Stukowski, A. Visualization and analysis of atomistic simulation data with OVITO−the Open Visualization Tool. *Modell. Simul. Mater. Sci. Eng.* **2010**, *18*, 015012.

(37) Umeda, K.; Kobayashi, K.; Minato, T.; Yamada, H. Atomic-level viscosity distribution in the hydration layer. *Phys. Rev. Lett.* **2019**, *122*, 116001.

(38) Hu, X.; Egberts, P.; Dong, Y.; Martini, A. Molecular dynamics simulation of amplitude modulation atomic force microscopy. *Nanotechnology* **2015**, *26*, 235705.

(39) Chelikowsky, J. R.; Fan, D.; Lee, A. J.; Sakai, Y. Simulating noncontact atomic force microscopy images. *Physical Review Materials* **2019**, *3*, 110302.

(40) Dzedzickis, A.; Bucinskas, V.; Viržonis, D.; Sesok, N.; Ulcinas, A.; Iljin, I.; Sutinys, E.; Petkevicius, S.; Gargasas, J.; Morkvenaite-Vilkonciene, I. Modification of the AFM sensor by a precisely regulated air stream to increase imaging speed and accuracy in the contact mode. *Sensors* **2018**, *18*, 2694.

(41) Peng, J.; Guo, J.; Hapala, P.; Cao, D.; Ma, R.; Cheng, B.; Xu, L.; Ondráček, M.; Jelínek, P.; Wang, E.; et al. Weakly perturbative imaging of interfacial water with submolecular resolution by atomic force microscopy. *Nat. Commun.* **2018**, *9*, 122.

(42) Fukuma, T.; Kobayashi, K.; Matsushige, K.; Yamada, H. True atomic resolution in liquid by frequency-modulation atomic force microscopy. *Appl. Phys. Lett.* **2005**, *87*, 034101.

(43) Voïtchovsky, K.; Kuna, J. J.; Contera, S. A.; Tosatti, E.; Stellacci, F. Direct mapping of the solid−liquid adhesion energy with subnanometre resolution. *Nat. Nanotechnol.* **2010**, *5*, 401−405.

(44) Fukuma, T. Improvements in fundamental performance of in-liquid frequency modulation atomic force microscopy. *Microscopy* **2020**, *69*, 340−349.

(45) Goral, M.; Wisniewska-Goclowska, B. IUPAC-NIST Solubility Data Series. 82: Alcohols with Water—Revised and Updated: Part 2. C 5 Alcohols with Water. *Journal of physical and chemical reference data* **2007**, *36*, 133−190.

(46) Albonetti, C.; Casalini, S.; Borgatti, F.; Floreano, L.; Biscarini, F. Morphological and mechanical properties of alkanethiol self-assembled monolayers investigated via bimodal atomic force microscopy. *Chem. Commun.* **2011**, *47*, 8823−8825.

(47) Yang, Y.; Bittner, A. M.; Baldelli, S.; Kern, K. Study of self-assembled triethoxysilane thin films made by casting neat reagents in ambient atmosphere. *Thin Solid Films* **2008**, *516*, 3948−3956.

(48) Ramin, L.; Jabbarzadeh, A. Effect of load on structural and frictional properties of alkanethiol self-assembled monolayers on gold: some odd−even effects. *Langmuir* **2012**, *28*, 4102−4112.

(49) Hanasaki, I.; Nakatani, A. Hydrogen bond dynamics and microscopic structure of confined water inside carbon nanotubes. *J. Chem. Phys.* **2006**, *124*, 174714.

(50) Valiokas, R.; Östblom, M.; Svedhem, S.; Svensson, S. C.; Liedberg, B. Thermal stability of self-assembled monolayers: Influence of lateral hydrogen bonding. *J. Phys. Chem. B* **2002**, *106*, 10401−10409.